EEET ECOLOGICAL ENGINEERING & ENVIRONMENTAL TECHNOLOGY

Ecological Engineering & Environmental Technology 2024, 25(9), 336–347
https://doi.org/10.12912/27197050/190862
ISSN 2299–8993, License CC-BY 4.0

Received: 2024.06.26
Accepted: 2024.07.10
Published: 2024.08.01

Performance of Graphene Oxide–Titanium Dioxide, Polyethersulphone Membranes for Industrial Wastewater Treatment

Zahraa Salah Jassim[1*], Auda Jabbar Braihi[1], Kadhum M. Shabeeb[2]

[1] Polymer and Petrochemical Industries Engineering Department, College of Engineering Materials, University of Babylon, Hilla, Iraq

[2] Materials Engineering Department, University of Technology, Baghdad, Iraq

* Corresponding author's e-mail: haydear879@gmail.com

ABSTRACT

The use of hydrophilic polymer membranes derived from nanocomposites for the treatment of industrial wastewaters has garnered significant attention lately. When producing membranes, the fouling problems of these membranes may be lessened by adding hydrophilic additives to the polymer solution. In order to create the membranes by the phase inversion approach, 0.8 weight percent of polyethersulfone (PES) solution was mixed with a combination (1:1) of graphene oxide:titanium dioxide nanoparticles (GO:TiO_2 NPs) at various weight percentages (0.2, 0.4, 0.6, and 0). The absence of spectral peaks at 899 and 1669 cm^{-1} in the completed membranes, as determined by FTIR studies, suggests that the GO:TiO_2 NPs component's hydrolytic breakdown caused the membrane structure's pores to develop. The membrane topology was rough with a wider range of heights and abnormalities at low NP concentrations, as the histogram of the 3D AFM pictures illustrates. On the other hand, the 2D photos showed that the surface smoothed out and had fewer peaks and valleys at high NP concentrations, which decreased the surface's roughness. Surface scanning electron microscopy pictures demonstrated that when the membrane's structure evolved from narrow to broad porosity with uneven expansion of porous patches, adding more nanoparticles increased the water flow. However, cross-sectional SEM pictures showed that the membrane's constituent parts were a thick porous layer with micropores and elongated finger structures that resembled pores, and a thin skin layer. The membrane's porosity increased with increasing NP concentration, as demonstrated by porosity calculations and contact angle measurements. This improved selectivity, made the membrane less prone to fouling, and made cleaning safer and easier, particularly for hydrophilic foulants like proteins and polysaccharides. The addition of NPs resulted in an estimated 83% and 92% increase in the flow of pure water and bovine serum albumin (BSA), respectively. However, the BSA rejection initially dropped before increasing once again.

Keywords: PES membrane, graphene oxide, titanium dioxide, pure water flux, bovine serum albumin rejection.

INTRODUCTION

Numerous companies release substantial amounts of industrial effluent into aquatic bodies, which is a major contaminant [Garg et al., 2022]. Treated wastewater is very hazardous to human health and ecosystems because of its toxicity and significant environmental concerns [Karriet et al., 2021].

Adsorption, dissolved air flotation, and conventional filtration are examples of physical treatment for wastewater, while chemical treatment includes chemical oxidation, emulsification lysis, and conventional filtering [Medeiros et al., 2022].

The creation of byproducts and the need for risky materials are drawbacks of those remedy techniques [Saravanan et al., 2021]. Because dangerous contaminants may additionally kill microorganisms due to their life, organic treatments are much less powerful at getting rid of refractory pollutants from wastewater than they may be at doing away with dissolved and suspended chemical compounds [Ata et al., 2021]. The charm of membrane techniques as a 21st century

era is expanded by those drawbacks [Tsehaye et al., 2022]. Wastewater remedy now has a sensible opportunity in membrane separation era. Reverse osmosis (RO), microfiltration (MF), ultrafiltration (UF), nanofiltration (NF), and microfiltration (MF) are the four number one categories of membrane technology [Maroufi and Hajilary, 2023].

The essential feature that distinguishes the various uses for those membranes is their pore length. Ultrafiltration has a excessive elimination performance, calls for no chemical additions, and uses less strength than earlier separation procedures [Ahmad et al., 2020]. One disadvantage of membrane remedy is membrane fouling, which appreciably lowers the membrane's water go with the flow efficacy [Wang et al., 2023]. When impurities within the water persist with the membrane's surface or move into its shape, fouling occurs. The solvent is not able to pass thru the membrane pores due to these contaminants. As a result, several processes to solving the fouling issue with polymer membranes have been devised [El Batouti et al., 2021].

Hydrophilic chemical addition to polymers is a beneficial remedy for this trouble. A latest studies shows that titanium oxide (TiO_2) and graphene oxide (GO) have drawn quite a few interest for his or her hydrophilicity and other favored capabilities in membrane technology [Oliveira et al., 2022]. GO may be integrated with polymer membranes to beautify mechanical power, reduce and maximize the possibility of organic and biofouling, and enhance floor hydrophilicity and water permeability by using floor functionalization or embedding inside the polymer matrix [Alkhouzaam and Qiblawey, 2021]. Nevertheless, the membrane may also collect hydrophilicity and photocatalytic pastime with the addition of TiO_2 [Covaliu-Mierlă et al., 2022]. The Novelty of the study is use of ideal nanomaterial GO/TiO_2 in the preparation of PES membrane to enhance its performance.

In this paintings, GO and TiO_2 had been incorporated into PES polymer at various ratios to create a polymer membrane with enhanced performance in phrases of pure water glide and BSA retention [Amiri et al., 2021]. Additionally, FTIR, AFM, SEM, in addition to measures of porosity and speak to attitude, were used to represent the membrane.

The purpose of the study is to raise the membrane's surface hydrophilicity which in turn reduce the fouling formation on membrane surface and increase the pure water flux of the membrane.

EXPERIMENTAL PART

Materials

Polyethersulfone (PES) is a polymer with a density of 1370 kg/m3 that was used as the matrix material for the membrane. The solvent, DMSO, originated in Belgium and had a density of 1.10 g/ml and molecular weight of 78.13 g/mol, DMSO has a distinct bitter taste and smell and is a clear, colorless to yellowish liquid. Saturated aliphatic compounds are practically insoluble in it, but it is soluble in water, ethanol, acetone, diethyl ether, benzene, and choro form. It is an excellent solvent for unsaturated, nitrogen-containing, and aromatic compounds. DMSO appears to have a relatively low order of systemic toxicity; however, it should not be used with strong oxidizing or reducing agents and should be stored in sealed containers due to its hygroscopic characteristic.

It is an important solvent due to its outstanding solvent capabilities and other qualities. Colorless, dimethyl sulfoxide (DMSO) was once employed as an industrial solvent. The substance is polar and easily blends with ethyl alcohol and a variety of organic solvents. It has a high hygroscopic capacity, absorbing almost 70% of its weight in water from the atmosphere. DMSO is an amphipathic molecule that is soluble in both organic and aqueous solutions. It has some antibacterial and antifungal activity. As a result, it has been applied in numerous scientific domains as a solvent and carrier for organic molecules.

PVP Molecular weight: 40,000g\mol Bought from: England Glentham life sciences company, In order to improve the properties and hydrophilicity of the membranes, PVP, a hydrophilic, biocompatible, and nontoxic polymer, is added to polymer solutions as pore-forming and structure-controlling agents. Fouling is less likely as a result. PVP contributes to the creation of holes and increases the water affinity of membranes. Known as a "pore agent" polymer dissolves in water to form pores in the membrane's structure. PVP, a highly hydrophilic polymer, is added to food to enhance the membrane's stabilizing and thickening properties. Surface stabilization is another function of PVP. While TiO_2 powder (anatase) obtained from Hongwu International Co., Ltd., had a molecular weight of 40,000 g/mol. Nano graphene oxide (GO) particles

obtained from Platonic Nanotech Private Limited have a diameter of 20 μm and purity at 99.9%, with less than 5nm thickness but size between 5–15 nm; Solarbio China is the source for bovine serum albumin (BSA), which has a molecular weight of 68000 g/mol.

Membrane preparation

This phase inversion method was used to construct the PES membrane. 17% PES, 1% PVP, and 82% DMSO were combined to create a polymer solution (Table 1). For a whole day, the mixture was swirled. Following that, various quantities of (1:1) TiO_2:GO were added in accordance with Table 1 and mixed once more for a whole day. After 30 minutes of sonication, the solution was transferred with a spatula onto a glass plate.The membrane was submerged in a coagulation bath of distilled water. Every two days, the distilled water used to maintain the membrane was changed. The membrane was then allowed to air dry before being kept for further analysis. These specific weight percentages of either GO or TiO_2 were chosen as a conclusion of previous studies on using this filler in membrane formulations for wastewater purification.

Membrane characterization

FTIR spectroscopy

In accordance with ASTM E1252, the chemical composition of the produced membranes was investigated using Fourier transform infrared spectroscopy (FTIR) in the 500–4000 cm^{-1} range

Scanning electron microscopy (SEM)

The VEGA3 LM -TESCAN apparatus, which utilizes liquid nitrogen to cut small pieces (0.5 × 0.5 cm) from the generated membrane, was used to conduct the test. After submerging the parts in liquid nitrogen for 60 to 90 seconds, they were frozen. The membrane's frozen portions were divided and kept separate until they air-dried.

Atomic force microscopy (AFM)

The generated membranes' surface morphology was investigated using an atomic force microscope (Naio AFM 2022, Nanosurf AG, Switzerland), and the Mountains SPIP® Academic 9.3.10249 technique was used to calculate the surface roughness parameters in accordance with ASTM E 2865.

Measurement of contact angle (CA)

In a circular fit mode, contact angle (CA) measurements were made to assess the hydrophilicity of the produced membranes. Because it lessens fouling and extends membrane life, hydrophilicity is a crucial factor to take into account in membrane applications. An Optical Dynamic I Static Interfacial Tensiometer and Contact Angle Meter (SL 200C) made in the United States by KINO Industry Co., Ltd. was the apparatus used. Range of contact angles: 0° to 180°. Double-sided tape was used to secure the membrane sample to a glass substrate. Next, five drops of 5 μL deionized water were placed at various positions on the membrane surface to measure the contact angle.

Porosity

The dry technique was used to assess the membrane's porosity. There was a 2 cm by 2 cm sample. The membrane sample's weight was determined. The following formula was used to calculate the membrane porosity [Sweet, 2014].

$$\varepsilon = 1 - \frac{\rho m}{\rho p} \times 100 \quad (1)$$

where: ε stands for porosity (%), ρm for membrane density (g/cm^3), and ρp for polymer density. This test was conducted using a density tester in accordance with ASTM D-792.

Table 1. Fabricated membrane components

Membrane symbol	PES (wt. %)	DMSO solvent (wt. %)	PVP (wt. %)	NPs (GO + TiO_2) (wt. %)
M_1	17	82	1	0.0
M_2	17	81.8	1	0.2
M_3	17	81.6	1	0.4
M_4	17	81.4	1	0.6
M_5	17	81.2	1	0.8

Membrane performance

With the use of a cross-flow mode on a laboratory scale, the membrane performance was examined. An active area of 12 cm^2 membrane cell formed part of the experimental setup. The formula below was used to calculate the PWF[Aaij et al., 2014].

$$J = \frac{V}{A \times t} \quad (2)$$

where: A is the effective area (m^2), V is the quantity of permeate collected during the operation period t (h) (m^3), and PWF is the pure water flow rate (often abbreviated as J) ($kg/h \cdot m^2$). Verify the BSA solution (1 g BSA/liter distilled water) and pure water flow rates. The following formula is used to calculate the BSA solution rejection. [de Carvalho et al., 2006]:

$$R\% = \left(1 - \frac{Cp}{Cf}\right) \times 100 \quad (3)$$

where: the BSA concentrations (mg/l) in the feed and permeate solutions are denoted by *Cp* and *Cf*, respectively. At a wavelength of 595 nm, *Cp* was measured using a UV-VIS spectrometer type UV-1100.

RESULTS AND DISCUSSION

FTIR results

Figure 2 depicts the impact of adding 1:1 GO:TiO_2 NPs, whereas Figure 1 displays the FTIR spectra of pure PES, GO, and TiO_2 materials.

The spectral features of PES membranes, whether or not GO:TiO_2 NPs are added, are indicated by the emergence of different absorption peaks. The peak at 1103.28 cm^{-1} represents the stretching of (C–O) bonds, whereas the corresponding peaks at 1242.16 cm^{-1} and 1149.57 cm^{-1} indicate the stretching of (C–O–C) bonds and (O–S–O) symmetric bonds. The results of the previous research by Hosseini and Alvi are supported by the following findings. Moreover, the peaks at around 1577.7 cm^{-1} and 1485.9 cm-1 are linked to the existence of aromatic rings, and the bond's peak at 3100 cm^{-1} is linked to the stretching of C-H bonds. The SO_2 molecule's scissor deformation is consistent with the spectral signature seen at 560 cm^{-1}. Furthermore, the SO^2 molecule stretches symmetrically and asymmetrically, producing peaks that are visible at 12.94 cm^{-1} and 1175 cm^{-1}, respectively. It is possible that the aryl-O-aryl C-O stretching mode is connected to the peak at 1244 cm^{-1}.

The following bands are seen for TiO_2: OH stretching is represented by the band at about 3400 cm^{-1}, Ti-OH vibrations are represented by the band at 1627.29 cm^{-1}, and Ti-O vibrations are represented by the band at 483.21 cm^{-1}. In GO, the C-O-C band is located at 1056.99 cm^{-1}, the C-OH band is located at 1188.15 cm^{-1}, and the band at 1620 belongs to C-OH.The band at 3417, 07 cm^{-1} represents the O-H voltage oscillation, and 21 cm^{-1} is part of the C = C group.

As shown in Figure 2, the absorption bands found in the spectra of PES/GO:TiO2 NPs and pure PES membranes exhibit the same properties [Mousa et al., 2023]. Furthermore, it is notable that the PES/GO:TiO_2 NPs membrane notably lacks the spectral peaks at 1669 and 899 cm^{-1}. These findings imply that the hydrolytic degradation process of the GO:TiO_2 NPs component causes notable alterations that eventually lead to

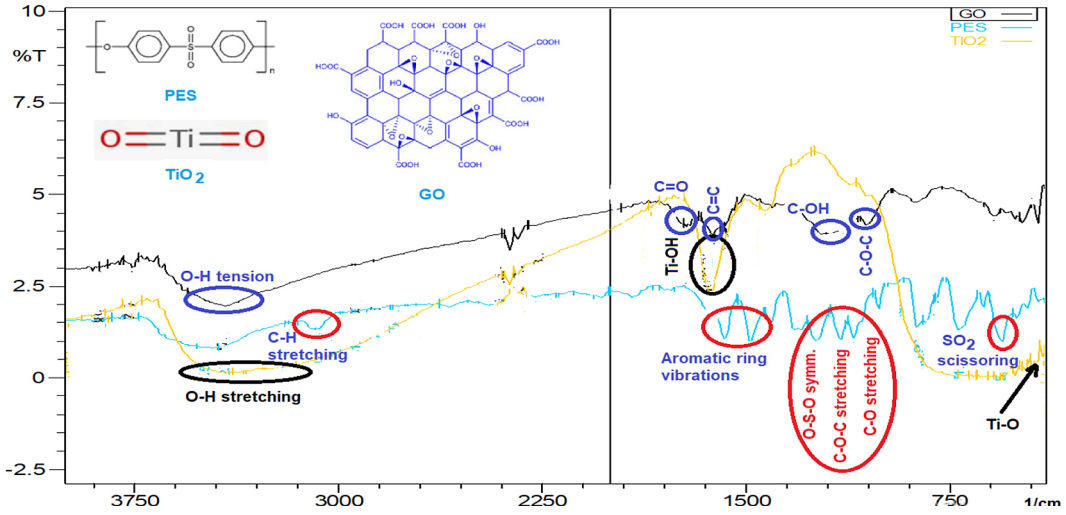

Figure 1. FTIR spectra for PES, GO and TiO_2

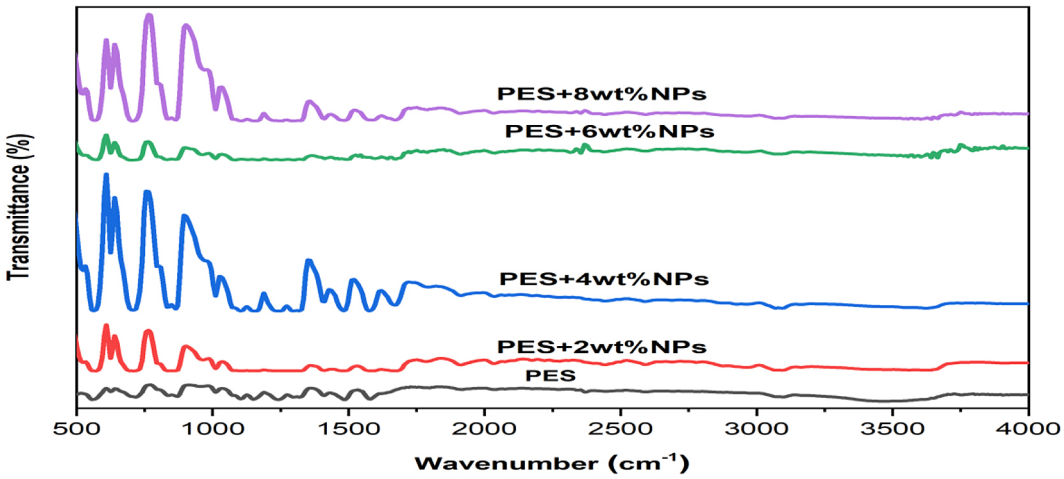

Figure 2. FTIR spectra of PES, GO:TiO_2 NPs and PES/GO:TiO_2 NPs

the creation of holes in the membrane structure. Due to the high concentration of hydroxyl (OH-) groups in the nanoparticle structure, one explanation for the observed degrading behavior might be addressed. These hydroxyl (OH-) groups aid in the creation of hydrogen bonds with water molecules in the coagulation bath [Guo et al., 2022].

Membrane morphology

The film morphology was investigated using scanning electron microscopy (SEM) and atomic force microscopy (AFM) [Buys et al., 2013].

Table 2 shows that when GO:TiO_2 is added, surface roughness initially rises to a certain point before falling and staying steady [Buys et al., 2013]. From 253.1 nm to 630.2 nm, the root mean square height (Sq) rises, falls to 145.9 nm, and then stays steady at this point. Other factors, such as the maximum height (Sz) and the arithmetic mean height (Sa), exhibit the similar trend [Somovilla-Gómez et al., 2020]. That is, a deeper valley and a greater departure from the center line occur when the addition quantity of GO:TiO_2 is minimal. Because the GO:TiO_2 particles are tougher and harder than the PES matrix, they protrude from the PES surface. This causes the average deviation from the center line to rise, which in turn increases the roughness parameters [Sinha Ray et al., 2020].

At higher additions, GO:TiO_2 filler become more uniformly distributed, filling the voids among PES chains and integrated with this polymeric matrix; thus the surface become smoother, with less peaks and valleys, leading to a decrease in the surface roughness [Farahbakhsh et al., 2021].

At certain GO:TiO_2 level, the surface roughness reach a stable state due to the balancing between the roughening effect of the GO:TiO_2 particle and the smoothening effect due to their unform distribution followed by integration. Fast stabilization occurred due to the following reasons:

1. The particle sizes of GO:TiO_2 are very small; in nano scale.
2. The distribution is uniform within the PES matrix.
3. There is some compatibility and adhesion interactions between the GO:TiO_2 particles and the PES chains.
4. The mixing conditions and the molding style (to form the membrane film) enhances the dispersion efficiency

Table 2. Several roughness attributes of the samples that were produced

Membrane symbol	S_q (nm)	S_a (nm)	S_z (nm)
M_1	253.1	224.5	990.7
M_2	479.5	410.3	1782
M_3	630.2	542.1	2356
M_4	145.9	123.4	639.8
M_5	145.9	123.4	639.8

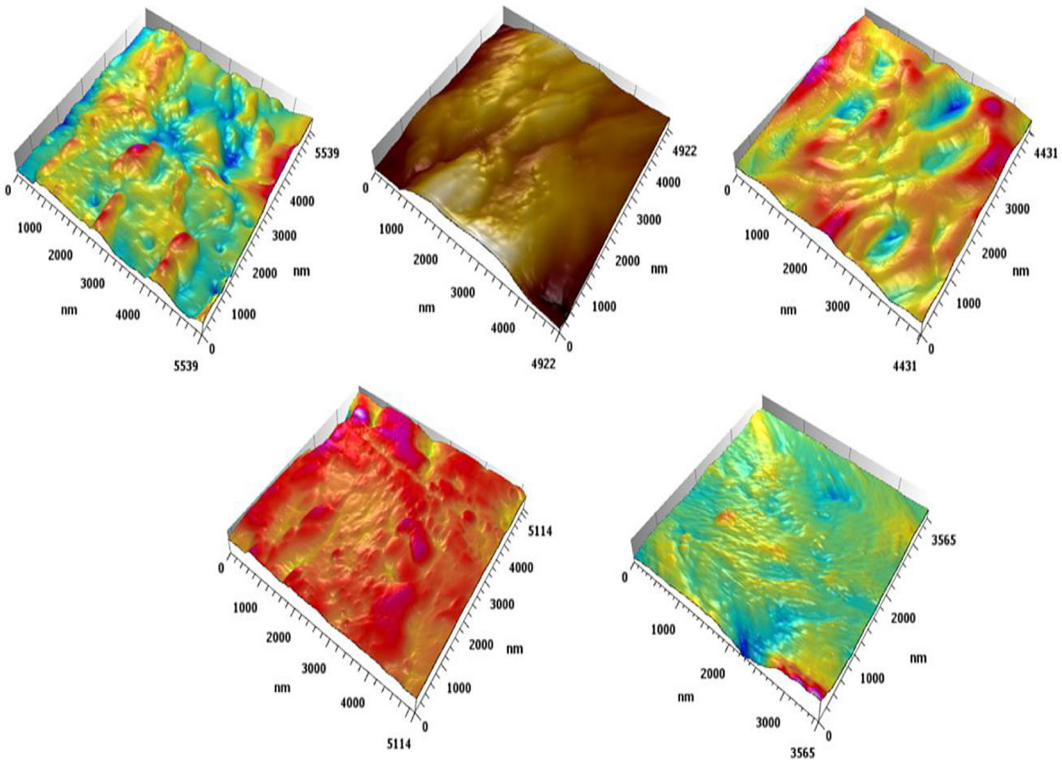

Figure 3. Histograms of the prepared membrans

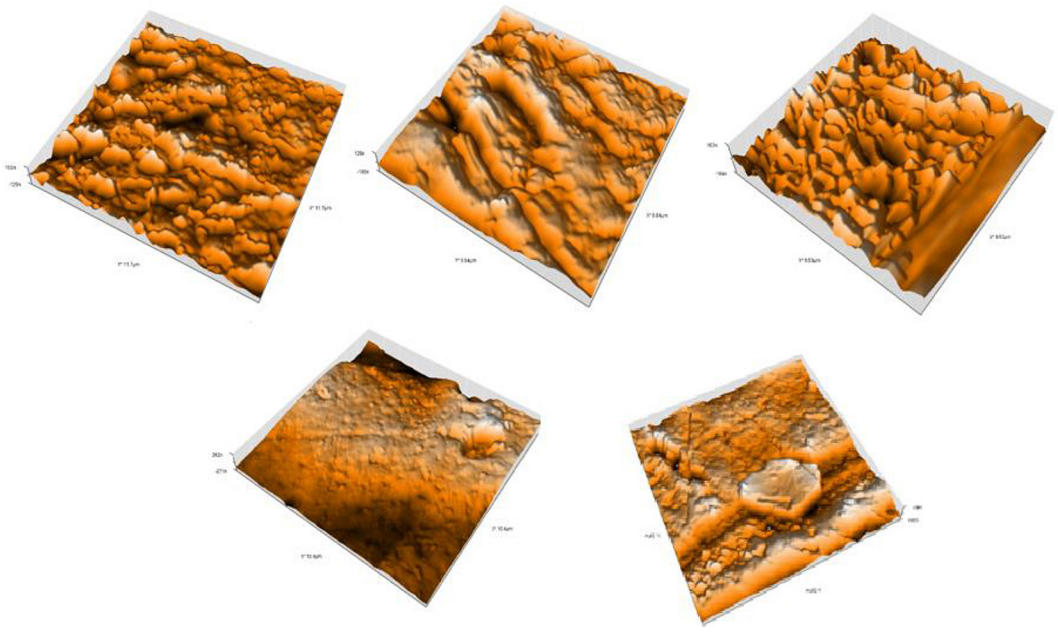

Figure 4. 2D AFM images of the prepared membrans

The same previous findings obtained from the histograms (Figure 3) and from the 2D AFM images (Figure 4). Histograms shows that at low GO:TiO_2 levels, the membranes topography are rough with wider spread of heights and irregulates. In the same context, the 2D AFM images shows that the membrane surface morphology contains many surface features, such as asperities, pits, valleys and peaks and these features decreased at high GO:TiO_2 levels.

The morphology of the produced membranes was examined using surface and cross-sectional SEM images (Figures 5 and 6). As the GO:TiO_2 loading increased, the surface pictures

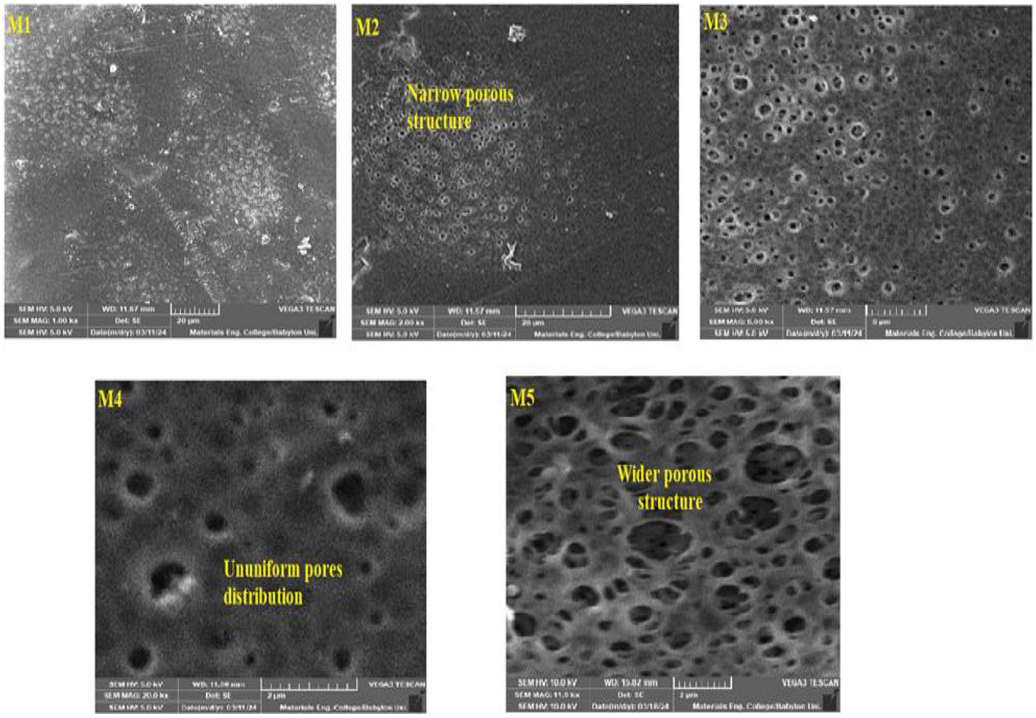

Figure 5. Surface pictures obtained by SEM of the constructed membranes

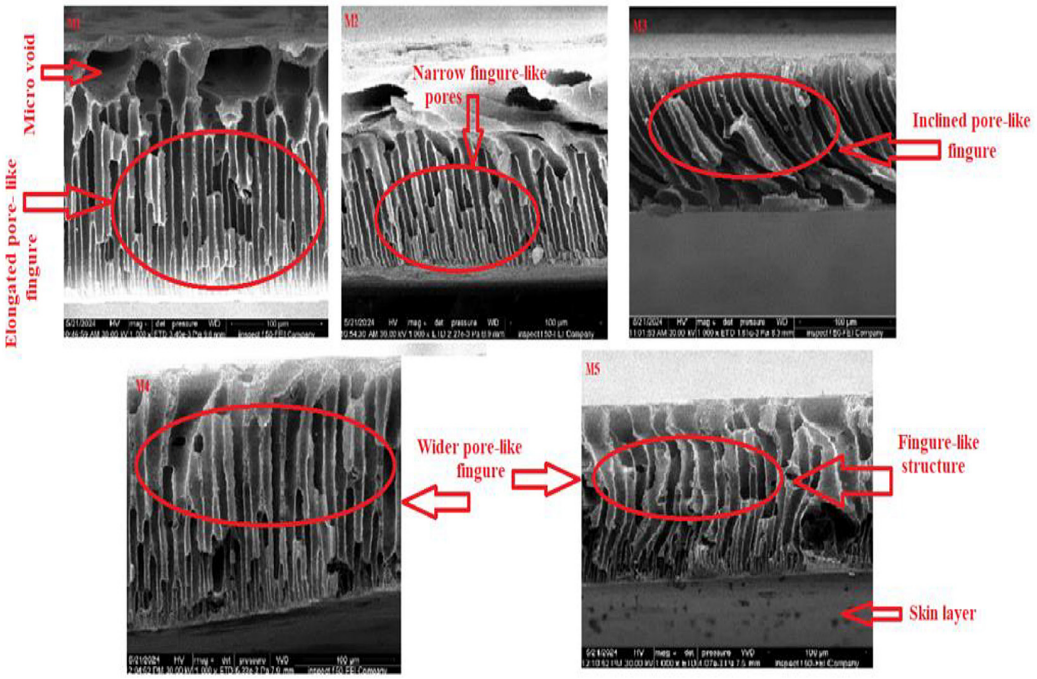

Figure 6. SEM pictures of the produced membranes in cross section

demonstrated that the membrane structure shifted from having narrow pores to having broader pores [Xu et al., 2017]. It is thus thought that this new structure would enhance water flow and eventually improve membrane performance since the porosity increased and was unevenly distributed [Zhang et al., 2021]. The membrane is comprised of two layers, as shown by cross-sectional SEM images: a layer with high porosity and a thin surface layer [Tiraferri et al., 2011]. Extended pores and microspaces make up the patterned structure of the bottom layer [Schutjajew et al., 2021]. These photos support earlier findings that added GO:TiO_2 causes fingers to enlarge.

Porosity results

As the GO:TiO_2 concentration rose, Figure 7 illustrates that the porosity increased as well, which is consistent with earlier morphological observations. It is anticipated that this porosity increment increased the treated water's (permeate's) flow rate, improving both productivity and the efficacy of removing contaminants [Shah et al., 2020]. High porosity reduced fouling and clogging, where membranes become less susceptible to fouling by solid particles and organic impuirities, which leads to reduce the maintenance periodic and increases the membrane lifspan [Gul et al., 2021]. Membrans with high porosity oftenly, require less operational pressure, which resulted in reduction of the energy consumption and saving cost [Judd, 2017]. Also, the increament in porosity can improve the selectivity twoards removing certain contiminates, while allowing the passage of the desired components, such as water molecules[Song et al., 2023]. Results showed at higer GO: TiO_2 level, there is some stability in the porosity values. Indeed, this is a desired behavior since the continuous increase in the porosity leads to reducing the mechanical strength and finally membrane damage [Kusworo et al., 2022]. Therefore, an optimal porosity is necessary to balancing the membrane performance with its lifespan.

Wettability results

Membrane wettability was evaluated through the contact angle measurments using circle fitting mode (Figure 8). Results showed that the contact angles are generally decrased as filler increased; the wattability increased and the mambrane be more hydrophilic [AbdulKadir et al., 2020]. This is a desired behavior in wastewater purification application where hydrophilic membranes have high affinity twords water molecules, which enhances the overall eficiency due to the increament in the permeat flux throuh the membrane [Ahmad et al., 2020].

Also, this membrane type has excellent efficiency in rejection polar and charged pollutants, such as salts and heavy metals [Castro-Muñoz et al., 2021]. This type, also, are less susceptible to the adsorption of impurities, which, otherwise with time resulted in formation of fouling layers upon the membrane surface. This can help in reducing the need for frequent cleaning [Gul et al., 2021].

In cleaning processes, hydrophilic membranes can be easily cleaned since they used water-base solutions, which depend on the penetration of water molecule and removing the accumulated impurities [Alipoori et al., 2021]. This water-based cleaning method considered environmentally friendly method since it avoids using harsh chemicals.

Hydrophilic foulants, like polysaccharides and proteins are more compatible with this membrane type; thus, these foulants can easily remove during cleaning process.

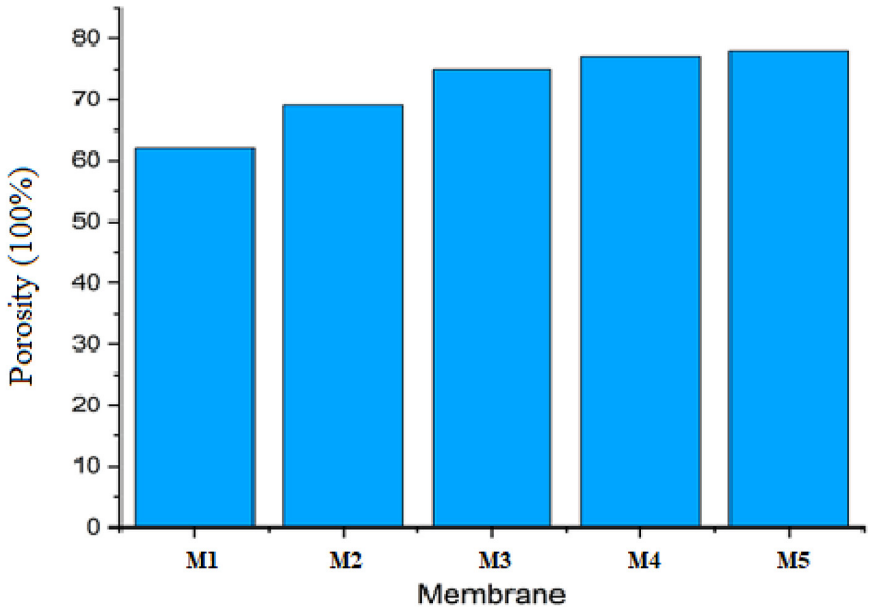

Figure 7. Membrans porosity as a function of GO: TiO_2 level

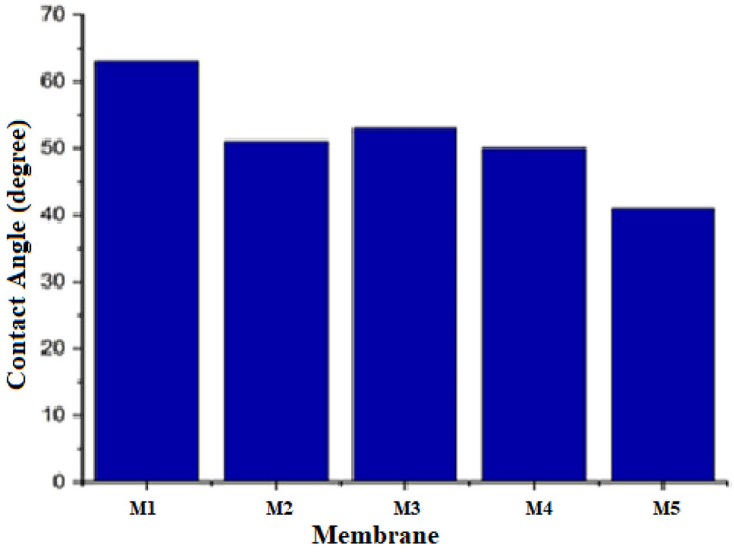

Figure 8. Membrans contact angles as a function of GO:TiO_2 level

Performance of membrane

Pure water flux (PWF)

Figure 9 shows the observed flow of pure water and diluted BSA solution (1000 ppm). The findings indicate that the ratio of GO:TiO_2 NPs grows linearly with the flow of pure water. The following factors account for this anticipated increase:

1. Increased hydrophilicity, or the ability of the membrane surface to attract water molecules.
2. A higher porosity.
3. Compared to a typical PES membrane, there are more vertically linked finger-like holes formed.
4. Hydrophilic particles accelerate the pace at which DMSO and water interchange during membrane growth, leading to a membrane that is more porous and has more holes. Consequently, the membrane's PWF and separation performance have increased.
5. The geometry of the membrane is significantly altered by hydrophilic nanoparticles. In particular, the initial PES membrane, which is made up of tiny holes the size of fingers, changes into larger pores linked to enormous PES gaps.
6. Less fouling and clogging propensity since impurities are less likely to cause the membrane to foul.

As a result of this modification, the water flow rate increased from 150 kg/h.m^2 to 275 kg/h·m^2,

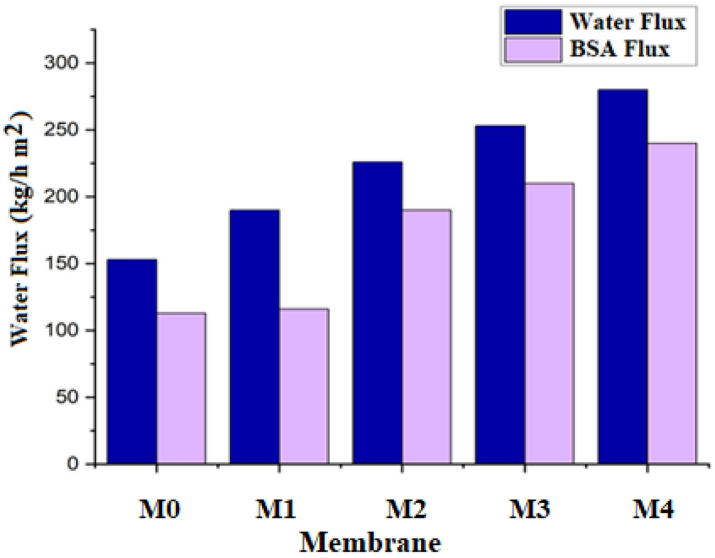

Figure 9. Fluxes of pure water and BSA solution as a function of GO: TiO_2 level

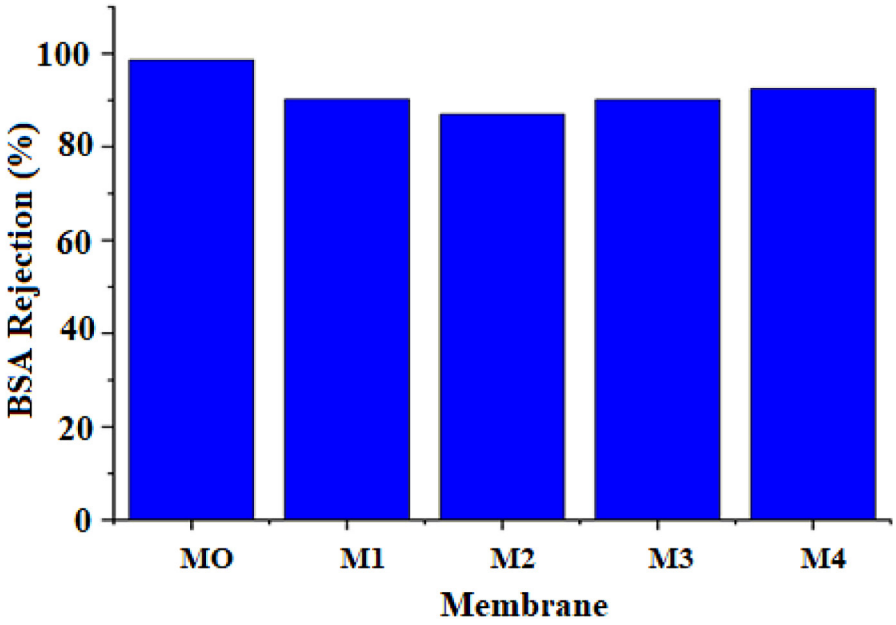

Figure 10. Bovine serum albumin rejection

boosting the PWF by about 83% and creating a more efficient pathway for water molecules to penetrate. The BSA solution produced the same results, albeit the flow rate values were lower [Babuet al., 2023]. This is because the water molecule (0.28 nm) is smaller in size than the BSA molecule (8–9 nm).

Albumin serum rejection

Bovine Serum Albumin (BSA) considered a good model for the rejection of proteins and other macromolecules by membranes, where the diameter of its molecule is about 8–9 nm, its molecule dimensions are ($14 \times 4 \times 4$ nm^3) and its molecular weight is 66.5 kDa (kilodalton) [Andersson, 2020]. Thus, using BSA as a standard can provide a good indication of the membrane's overall performance in retaining desired solutes.

Figure 10 showed that the rejection ability to BSA solution decreased slightly at low NPs levels (compared with the neat membrane), then increased at higher NPs levels. At low NPs levels, there is some phase separation between the PES polymeric chain and the solid NPs particles, which create paths to BSA molecules to passage through the membrane structure[Tehrani et al., 2023]. In contrast, at higher NPs levels, the BSA rejection (R%) increased due to:

1. NPs particles occupied voids among PES chain, allowing to less amounts of BSA molecules to pass.
2. High NPs levels increases the hydrophilicity of the membrane surface, may be responsible for the rise in rejection for these membranes.
3. Membrane rejection may have increased as a result of that albumin serum molecules' decreased affinity and interactions with the membrane surface.
4. As NP levels rise, so does the repulsive force between the membrane and BSA. Aspartic acid and glutamic acid, among other amino acids, ionize on the surface of BSA, giving it a pure negative charge. TiO_2 molecules are neutral, however there is a significant negative charge in the (1:1) combination GO:TiO_2 NP. Because of the functional groups that include oxygen on its surface, GO has a negative charge [Nebol'Sin et al., 2020].

CONCLUSIONS

1. GO:TiO_2 NPs component underwent a hydrolytic breakdown, resulting in a notable modification, which leads to creation of pores in the membrane's structure.
2. With high GO:TiO_2 level, the surface becomes smoother, with less peaks and valleys, leading to a decrease in the surface roughness.
3. According to surface SEM images, it is expected an increment in the water flux, where the membrane structure converted from narrow porous structure to wider one and the porous be enlarged with ununiformed distribution. Cross-section morphology proved that membranes consist from thin skin layer and thick porous

layer, which includes micro voids and narrow elongated pore-like fingure structure.
4. With increasing the NPs level, the porosity increased and the membranes become more hydrophilic with less fouling tendicy and improved selectivity. According to the wettability results, with NPs level, membranes be possess higher affinity to water molecules and the cleaning process be easier and safer.
5. Hydrophilic dirt composed of polysaccharides and proteins is easily removed during the cleaning process due to its compatibility with the membrane structure.
6. As NPs levels increased, as pure water or BSA fluxes increased, while there is some fluctuation in the BSA rejection.
7. (a) the concentration of GO-TiO_2 between 0 and 0.8% while PES concentration was 17%; (b) pure water flux and BSA rejection were measured under operating pressure difference of 1 bar; (c) feed concentration of BSA was 1000 ppm.

REFERENCES

1. Garg, S., Chowdhury, Z.Z., Faisal, A.N.M., Rumjit, N.P., Thomas, P. 2022. Impact of industrial wastewater on environment and human health. Advanced Industrial Wastewater Treatment and Reclamation of Water: Comparative Study of Water Pollution Index during Pre-industrial, Industrial Period and Prospect of Wastewater Treatment for Water Resource Conservation, 197–209.
2. Karri, R.R., Ravindran, G., Dehghani, M.H. 2021. Wastewater—sources, toxicity, and their consequences to human health. In Soft computing techniques in solid waste and wastewater management. Elsevier, 3–33.
3. Medeiros, A.D.L.M.D., Silva Junior, C.J.G.D., Amorim, J.D.P.D., Durval, I.J.B., Costa, A.F.D.S., Sarubbo, L.A. 2022. Oily wastewater treatment: methods, challenges, and trends. Processes, 10(4), 743.
4. Saravanan, A., Kumar, P.S., Jeevanantham, S., Karishma, S., Tajsabreen, B., Yaashikaa, P.R., Reshma, B. 2021. Effective water/wastewater treatment methodologies for toxic pollutants removal: Processes and applications towards sustainable development. Chemosphere, 280, 130595.
5. Ata, R., Merdan, G.F., Töre, G.Y. 2021. Activated sludge process for refractory pollutants removal. In Removal of Refractory Pollutants from Wastewater Treatment Plants. CRC Pres,137–184.
6. Tsehaye, M.T., Assayie, A.A.Y., Besha, A.T.Y., Tufa, R.A.Y., Gebreyohannes, A.Y.Y. 2022. Membrane technology for water and wastewater treatment in Ethiopia: Current status and future prospects. Journal of Membrane Science and Research, 8(1).
7. Maroufi, N., Hajilary, N. 2023. Nanofiltration membranes types and application in water treatment: a review. Sustainable Water Resources Management, 9(5), 142.
8. Ahmad, T., Guria, C., Mandal, A. 2020. A review of oily wastewater treatment using ultrafiltration membrane: A parametric study to enhance the membrane performance. Journal of Water Process Engineering, 36, 101289.
9. Wang, Q., Lin, W., Chou, S., Dai, P., Huang, X. 2023. Pattern membrane for improving hydrodynamic properties and mitigating membrane fouling in water treatment: A review. Water Research, 119943.
10. El Batouti, M., Alharby, N.F. Elewa, M.M. 2021. Review of new approaches for fouling mitigation in membrane separation processes in water treatment applications. Separations, 9(1), 1.
11. Oliveira, C.P.M., Farah, I.F., Koch, K., Drewes, J.E., Viana, M.M., Amaral, M.C.S. 2022. TiO_2-Graphene oxide nanocomposite membranes: a review. Separation and Purification Technology, 280, 119836.
12. Alkhouzaam, A., Qiblawey, H. 2021. Functional GO-based membranes for water treatment and desalination: Fabrication methods, performance and advantages. A review. Chemosphere, 274, 129853.
13. Covaliu-Mierlă, C.I., Matei, E., Stoian, O., Covaliu, L., Constandache, A.C., Iovu, H., Paraschiv, G. 2022. TiO_2–based nanofibrous membranes for environmental protection. Membranes, 12(2), 236.
14. Amiri, S., Asghari, A., Vatanpour, V., Rajabi, M. 2021. Fabrication of chitosan-aminopropylsilane graphene oxide nanocomposite hydrogel embedded PES membrane for improved filtration performance and lead separation. Journal of Environmental Management, 294, 112918.
15. Sweet, W.J. 2014. Application of Conductive Thin Films and Selectively Patterned Metal Oxide Coatings on Fibers by Atomic Layer Deposition.
16. Aaij, R., Adeva, B., Adinolfi, M., Affolder, A., Ajaltouni, Z., Akar, S.,... & De Simone, P. 2014. Measurement of the B^-0–B0 and B^-s0–Bs0 production asymmetries in pp collisions at s = 7 TeV. Physics Letters B, 739, 218–228.
17. de Carvalho, C.C., de Souza, M.P., da Silva, T.D., Gonçalves, L.A.G., Viotto, L.A. 2006. Soybeans crude oil miscella degumming utilizing ceramic membranes: transmembrane pressure and velocity effects. Desalination, 200(1–3), 543–545.
18. Mousa, S.A., Abdallah, H., Ibrahim, S.S., Khairy, S.A. 2023. Enhanced photocatalytic properties of graphene oxide/polyvinylchloride membranes by incorporation with green prepared SnO_2 and TiO_2

nanocomposite for water treatment. Applied Physics A, 129(12), 831.

19. Guo, K., Wang, Z., Pan, J., Liu, B., Wang, Y., Yue, Q., Gao, Y., Gao, B. 2022. Highly efficient Al-Ti gel as a coagulant for surface water treatment: Insights into the hydrolysate transformation and coagulation mechanism. Water Research, 221, 118826.
20. Buys, A.V., Van Rooy, M.J., Soma, P., Van Papendorp, D., Lipinski, B., Pretorius, E. 2013. Changes in red blood cell membrane structure in type 2 diabetes: a scanning electron and atomic force microscopy study. Cardiovascular diabetology, 12, 1–7.
21. Buys, A.V., Van Rooy, M.J., Soma, P., Van Papendorp, D., Lipinski, B., Pretorius, E. 2013. Changes in red blood cell membrane structure in type 2 diabetes: a scanning electron and atomic force microscopy study. Cardiovascular diabetology, 12, 1–7.
22. Somovilla-Gómez, F., Lostado-Lorza, R., Corral-Bobadilla, M., Escribano-García, R. 2020. Improvement in determining the risk of damage to the human lumbar functional spinal unit considering age, height, weight and sex using a combination of FEM and RSM. Biomechanics and modeling in mechanobiology, 19, 351–387.
23. Sinha Ray, S., Singh Bakshi, H., Dangayach, R., Singh, R., Deb, C.K., Ganesapillai, M., Chen, S.S., Purkait, M.K. 2020. Recent developments in nanomaterials-modified membranes for improved membrane distillation performance. Membranes, 10(7), 140.
24. Farahbakhsh, J., Vatanpour, V., Khoshnam, M., Zargar, M. 2021. Recent advancements in the application of new monomers and membrane modification techniques for the fabrication of thin film composite membranes: A review. Reactive and Functional Polymers, 166, 105015.
25. Xu, H., Ding, M., Liu, S., Li, Y., Shen, Z., Wang, K. 2017. Preparation and characterization of novel polysulphone hybrid ultrafiltration membranes blended with N-doped GO/TiO_2 nanocomposites. Polymer, 117, 198–207.
26. Zhang, W. H., Yin, M. J., Zhao, Q., Jin, C. G., Wang, N., Ji, S., Rit, C.L., Elimelech E.M., An, Q.F. 2021. Graphene oxide membranes with stable porous structure for ultrafast water transport. Nature Nanotechnology, 16(3), 337–343.
27. Tiraferri, A., Yip, N.Y., Phillip, W.A., Schiffman, J.D., Elimelech, M. 2011. Relating performance of thin-film composite forward osmosis membranes to support layer formation and structure. Journal of membrane science, 367(1–2), 340–352.
28. Schutjajew, K., Pampel, J., Zhang, W., Antonietti, M., Oschatz, M. 2021. Influence of pore architecture and chemical structure on the sodium storage in nitrogen-doped hard carbons. Small, 17(48), 2006767.
29. Shah, A.I., Dar, M.U.D., Bhat, R.A., Singh, J.P., Singh, K., Bhat, S.A. 2020. Prospectives and challenges of wastewater treatment technologies to combat contaminants of emerging concerns. Ecological Engineering, 152, 105882.
30. Gul, A., Hruza, J., Yalcinkaya, F. 2021. Fouling and chemical cleaning of microfiltration membranes: A mini-review. Polymers, 13(6), 846.
31. Judd, S.J. 2017. Membrane technology costs and me. Water research, 122, 1–9.
32. Song, Y., Phipps, J., Zhu, C., Ma, S. 2023. Porous materials for water purification. Angewandte Chemie, 135(11), e202216724.
33. Kusworo, T.D., Kumoro, A.C., Aryanti, N., Utomo, D.P., Hasbullah, H., Lingga, F. F., Yulfarida, M., Dalanta, F., Kurniawan, T.A. 2022. Photocatalytic antifouling nanohybrid polysulfone membrane using the synergetic effect of graphene oxide and SiO_2 for effective treatment of natural rubber-laden wastewater. Journal of Membrane Science, 657, 120663.
34. AbdulKadir, W.A.F.W., Ahmad, A.L., Seng, O.B., Lah, N.F.C. 2020. Biomimetic hydrophobic membrane: A review of anti-wetting properties as a potential factor in membrane development for membrane distillation (MD). Journal of Industrial and Engineering Chemistry, 91, 15–36.
35. Ahmad, T., Guria, C., Mandal, A. 2020. A review of oily wastewater treatment using ultrafiltration membrane: A parametric study to enhance the membrane performance. Journal of Water Process Engineering, 36, 101289.
36. Castro-Muñoz, R., González-Melgoza, L.L., García-Depraect, O. 2021. Ongoing progress on novel nanocomposite membranes for the separation of heavy metals from contaminated water. Chemosphere, 270, 129421.
37. Gul, A., Hruza, J., Yalcinkaya, F. 2021. Fouling and chemical cleaning of microfiltration membranes: A mini-review. Polymers, 13(6), 846.
38. Alipoori, S., Rouhi, H., Linn, E., Stumpfl, H., Mokarizadeh, H., Esfahani, M.R., Wujcik, E.K. 2021. Polymer-based devices and remediation strategies for emerging contaminants in water. ACS Applied Polymer Materials, 3(2), 549–577.
39. Babu, K.S., Amamcharla, J.K. 2023. Effect of bulk nanobubbles on ultrafiltration membrane performance: Physiochemical, rheological, and microstructural properties of the resulting skim milk concentrate dispersions. Journal of Food Engineering, 337, 111238.
40. Andersson, J. 2020. Interpolymer complexation of a polymer brush (Doctoral dissertation, Chalmers Tekniska Hogskola (Sweden)).
41. Tehrani, S.F., Bharadwaj, P., Chain, J.L., Roullin, V.G. 2023. Purification processes of polymeric nanoparticles: How to improve their clinical translation?. Journal of Controlled Release, 360, 591–612.
42. Nebol'Sin, V.A., Galstyan, V., Silina, Y.E. 2020. Graphene oxide and its chemical nature: Multi-stage interactions between the oxygen and graphene. Surfaces and Interfaces, 21, 100763.